Computational prediction of the fatigue behavior of additively manufactured porous metallic biomaterials

Hedayati, R.; Hosseini-Toudeshky, H; Sadighi, M.; Mohammadi-Aghdam, M.; Zadpoor, A. A.

DOI
10.1016/j.ijfatigue.2015.11.017

Publication date
2016

Document Version
Accepted author manuscript

Published in
International Journal of Fatigue

Computational prediction of the fatigue behavior of additively manufactured porous metallic biomaterials

R. Hedayati, H. Hosseini-Toudeshky, M. Sadighi, M. Mohammadi Aghdam, A.A. Zadpoor

PII: S0142-1123(15)00407-7
DOI: http://dx.doi.org/10.1016/j.ijfatigue.2015.11.017
Reference: JIJF 3784

To appear in: *International Journal of Fatigue*

Received Date: 24 August 2015
Revised Date: 15 November 2015
Accepted Date: 17 November 2015

Please cite this article as: Hedayati, R., Hosseini-Toudeshky, H., Sadighi, M., Mohammadi Aghdam, M., Zadpoor, A.A., Computational prediction of the fatigue behavior of additively manufactured porous metallic biomaterials, *International Journal of Fatigue* (2015), doi: http://dx.doi.org/10.1016/j.ijfatigue.2015.11.017

Original article

Computational prediction of the fatigue behavior of additively manufactured porous metallic biomaterials

R. Hedayati[1, 2*], H. Hosseini-Toudeshky[3], M. Sadighi[1], M. Mohammadi Aghdam[1], A.A. Zadpoor[2]

[1]*Department of Mechanical Engineering, Amirkabir University of Technology (Tehran Polytechnic), Hafez Ave, Tehran, Iran*
[2]*Department of Biomechanical Engineering, Faculty of Mechanical, Maritime, and Materials Engineering, Delft University of Technology (TU Delft), Mekelweg 2, 2628 CD, Delft, The Netherlands*
[3]*Department of Aerospace Engineering, Amirkabir University of Technology (Tehran Polytechnic), Hafez Ave, Tehran, Iran*

[1] Corresponding author, email: r.hedayati@tudelft.nl, rezahedayati@aut.ac.ir, rezahedayati@gmail.com, Tel: +31-15-2781021.

Abstract

The mechanical behavior of additively manufactured porous biomaterials has recently received increasing attention. While there is a relatively large body of data available on the static mechanical properties of such biomaterials, their fatigue behavior is not yet well-understood. That is partly because systematic study of the fatigue behavior of these porous biomaterials is time-consuming and expensive due to the large number of involved factors. In the current study, we propose a computational approach based on finite element method that could be used to predict the fatigue behavior of porous biomaterials given their type of repeating unit cell, dimensions of the unit cell, and S-N curve of the parent material. We applied the proposed approach to predict the fatigue behavior of porous titanium alloy (Ti-6Al-4V) biomaterials manufactured using selective laser melting based on the rhombic dodecahedron unit cell and compared our computational results with experimental observations from one of our recent studies. The evolution of the displacement, elastic modulus, and number of failed struts vs. the number of loading cycle followed a two-stage pattern. In the first stage, there was a relatively slow rate of change in the above-mentioned variables, while they changed very rapidly in the second stage. That compares to the behavior observed in our experimental study. The computationally predicted S-N curve well matched the experimental observations for stress levels not exceeding 60% of the yield stress of the porous structures. For higher stress levels, the presented approach substantially underestimated the fatigue life of the porous structures. The effects of the irregularities caused by the additive manufacturing process on the fatigue behavior of the porous structures were also studied. It was found that those irregularities substantially decrease the fatigue life particularly for lower stress levels.

Keywords: Fatigue behavior; Finite element; Porous titanium; Additive manufacturing.

1. INTRODUCTION

Bone possesses the intrinsic capacity of regeneration as a part of the repair process in response to injury [1, 2]. In specific clinical conditions such as large bony defects, this natural repair process cannot fully bridge the bony defect without the help of bone grafts. Autologous bone grafts (often harvested from the patient's iliac crest) is known as the gold standard treatment for treatment of such bony defects. However, autologous bone grafting is associated with well-known problems such as limited available bone stock and donor-site morbidity. Moreover, autologous bone grafting procedures usually have high complication rates including hemorrhage, nerve and vascular lesions, and post-operative pains [3]. Synthetic bone substitutes are therefore being constantly researched as alternatives.

One of the promising candidates for applications as bone substitute is open-cell porous metallic biomaterials. Those carefully designed and manufactured porous structures have several advantages over traditional solid implants. First, the micro-architecture of the porous structures could be designed such that the high elastic modulus of metallic biomaterials such as titanium alloys is decreased to levels comparable with bone [4, 5]. Second, the porous structures provide space for bone ingrowth and implant fixation. Third, the porous structures have a much larger surface area which is a golden opportunity in terms of surface treatments and coatings [6]. Finally, the open pore space could be used for delivery of drugs that stimulate bone regeneration and vascularization [7] and/or the ones that prevent infection.

Recently, additive manufacturing (AM) techniques including selective electron beam melting [8], selective laser sintering [9], and selective laser melting (SLM) [10-13] have enabled production of highly porous interconnected structures with arbitrary pore shapes and pore sizes in the range of $100 - 200\,\mu m$. Thanks to the manufacturing flexibility offered by AM

techniques, there has been enormous recent interest in additively manufactured porous biomaterials.

There is one major challenge when using highly porous metallic biomaterials which relates to the substantially decreased fatigue resistance of the porous structures as compared to the parent material. In one of our previous animal studies, we detected what seemed to be fatigue failure in the additively manufactured porous titanium implants that were used to graft critical-sized defects in the femurs of male Wistar rats [3]. Subsequent fatigue tests demonstrated that the fatigue resistance and endurance limits of additively manufactured porous structures are highly dependent on the type of unit cell and porosity [14, 15] and are critical factors that need to be carefully studied prior to application of porous biomaterials in large animal models and humans.

Most of the previous studies on the fatigue behavior of open-cell metal foams [16-21] and additively manufactured lattice structures [13, 22, 23] have been purely experimental. Experimental study of the fatigue behavior is extremely time-consuming and expensive, as many samples need to be tested under fatigue for extended periods of time. Numerical approaches that could be used to at least partially replace experiments are therefore very attractive. There are only a very limited number of numerical studies of the fatigue response of open-cell lattice structures. Although some studies exists in which Fracture Mechanics approaches have been used [24-28] to study the micromechanical crack propagation or fracture toughness of lattice structures, numerical prediction of the fatigue behaviour of additively manufactured porous structures based on the fatigue-life (or S-N diagram) method is not yet extensively performed. In a recent work, Demiray et al. [29] have analyzed the fatigue damage accumulation and failure of open-cell Kelvin metal foams using a computational approach. However, no quantitative validation of the computational results was performed in their study.

The aim of the current study is to present a computational approach that could be used for prediction of the S-N curve of additively manufactured porous biomaterials given the type of unit cell, the dimensions of the unit cell, and the fatigue behavior of the parent material. The main complexities and problems associated with such a study are presented and discussed. We also aim to fully validate our computational results by comparing them with the experimental data we obtained for the same porous structures in our previous studies. The effects of the irregularities and initial damages caused by the manufacturing process (Figure 1) on the static and fatigue behavior of additively manufactured porous structures are also studied.

2. MATERIALS AND METHODS

Porous titanium alloy (Ti6Al4V-ELI) structures based on rhombic dodecahedron repeating unit cell and manufactured using selective laser melting method were considered. Finite element (FE) models were created to analyze the static and fatigue behavior of the porous structures under compression. The computational results were validated with experimental data from one of our previous studies [15].

2.1. Creation of lattice structure

Creation of large lattice structures for FE study can be challenging. If a single unit cell with all its struts is going to be repeated in the three main directions of space to make a lattice structure, adjacent cells will have several coincident cell edges. The overlapping of the common edges of the adjacent cells could artificially stiffen the porous structure, leading to incorrect results. To overcome this problem, after creating each new unit cell, all possible overlaps with already existing unit cells were checked and removed.

2.2. Static behavior of the porous biomaterials

The elastic properties of Ti6Al4V-ELI (Table 1) were adopted for modeling the mechanical behavior of the parent material. The geometry of the porous structures modeled in this study including the specimens dimensions, pore size, strut diameter, etc. are the same as the ones used in our previous experimental study [15] (Table 2).

The lattice structures were discretized using Timoshenko beam elements. An implicit FE solver (ANSYS) was used for solving the governing equations of deformation. The actual boundary conditions experienced during mechanical testing were implemented in the model as two rigid plates positioned under and above the porous structures (Figure 2). More info on the modeling procedure for the static investigation can be found in [30, 31]. The irregularities caused by the additive manufacturing process, i.e. variations in the diameters of the struts, were implemented in the FE model in a way similar to what we described before [32]. The struts were discretized using several beam elements with variable diameters. The diameters of each of the beam elements were taken from a Gaussian distribution whose mean was the same as the strut nominal (i.e. design) diameter and its standard deviation was the same as what was found experimentally [15].

2.3. Fatigue behavior of the porous structures

Compression-compression fatigue simulations were carried out for the four porous structures listed in Table 2. Five different stress levels were applied to each porous structure. The load amplitudes were chosen such that the applied stress levels (the maximum applied compressive stresses to the structure) were between $0.2\ \sigma_y$ and $0.6\ \sigma_y$, where σ_y is the yield stress of each porous structure. The porous structures were assumed to have failed once the stiffness of the specimen dropped by more than 90%. S-N diagrams were used for stress-based fatigue-life

assessment and modeling the fatigue behavior of the porous structures and progressive failure analysis.

The S-N curve of Ti6Al4V in a completely reversible loading condition (Figure 3) was used to describe the fatigue behavior of the parent material. In the low-cycle part (i.e. cycle numbers smaller than 3×10^4), the LogS-LogN diagram of the parent material was assumed to be a straight line from point A (shown in Figure 3) to point $(0, LogS_u)$ [33]. Point A (the intersection point of high-cycle and low-cycle parts of the S-N curve) is called the intersection point in this paper. The endurance limit was considered 650 MPa [23].

2.3.1. Number of solution cycles

Fatigue simulations are usually computationally expensive because the simulation has to be repeated many times. Ideally, the cyclic simulations have to be repeated N times, where N is the number of cycles it takes for the porous structures to fail. However, to reduce the computational time, the number of simulation cycles could be smaller than the number of loading cycles. In fact, each simulation cycle can represent a number of loading-unloading cycles, Δn_i. A very large Δn_i can lead to inaccurate results, because the simulations cannot capture the gradual damage propagation in different parts of the lattice structure. On the other hand, a very small Δn_i can lead to a very long computational time. One of the very early steps of the problem was to find the optimum range of Δn_i based on a trial-and-correction approach.

2.3.2. Stress concentration factor

Irregularities created in the cross-section of the struts during additive manufacturing process decrease the structurual stiffness, compressive strength, and durability of the porous structures not only because they create cross-sections with very small areas, but also because they cause stress concentration. Roughness of strut surfaces results in local heterogeneities and stress

concentrations. Due to the very random distribution of roughness at different struts of an additively manufactured porous structure (as well as along each of the struts themselves), the stress concentration factors in different locations of the structure may be very different. However, we used one single stress concentration factor, K_f, for each type of porous structure, because no data regarding the statistical distribution of the stress concentration factors is currently available. To apply the stress concentration concept to the fatigue problem, after solving each simulation step, the obtained stress of each strut was multiplied by K_f before being used in the damage accumulation formulas. For each structure, first an arbitrary K_f was considred for the applied stress of $0.2\ \sigma_y$ and the fatigue life was obtained. The K_f value was then modified to find the K_f value which resulted in a fatigue life close to the experimental observations. The obtained K_f for $0.2\ \sigma_y$ was then also used for the four other stress levels, i.e. $\sigma = 0.3\ \sigma_y$, $0.4\ \sigma_y$, $0.5\ \sigma_y$, and $0.6\ \sigma_y$.

2.3.3. The effects of the deterioration of the elastic properties on fatigue behavior

Due to cyclic loading, damage is accumulated in different struts of the structure. In each loading-unloading cycle, the struts in which the degree of damage has reached a critical threshold fail. As the struts of the porous structure fail one by one during a cyclic loading, they lose their contribution to the load-bearing capacity of the lattice structure, thereby decreasing the stiffness of the structure. However, decrease in the stiffness of the lattice structure during a cyclic loading can also be due to the accumulation of damage in the struts of the structure even before they fail. According to the strain equivalence postulate [34, 35], the constitutive equation of a damaged material can be obtained by replacing the stress of the virgin material σ by the effective stress $\tilde{\sigma} = \sigma/(1 - D)$, where $\tilde{\sigma}$ is the force divided by the area that effectively sustains the load and D

is the accumulated damage in the material. Consequently, the elastic modulus of a damaged materials is given as [36]:

$$\tilde{E}_{i,j} = E(1 - \mathrm{D}_{i,j}) \quad (1)$$

where $E_{i,j}$ is the elastic modulus of strut i and $D_{i,j}$ is the accumulated damage to strut i (both corresponding to the simulation cycle j). Twenty different elastic moduli ranging from 0 to the initial value of the elastic modulus of the material, E_s, were defined and assigned to each strut at each simulation step according to the damage level of the strut (using Equation (1)).

2.3.4. The effects of initial damage

In the process of creation of a porous structure using additive manufacturing techniques, a few severely defected struts can be created. Those struts fail in the very early stages of the deformation of the porous structure and may not therefore contribute to the load bearing capacity of the structure. Effect of those struts on the fatigue behavior of the structure can be important and were therefore studied. To model the initially defected struts, the elastic modulus of some of the struts of the lattice structure (the location distribution of which was chosen randomly) was set to a negligibly small value, i.e. 1 Pa. The percentage of the damaged struts was varied to study the effect of the initial damage on the fatigue response of the porous structures.

2.3.5. The damage propagation algorithm

The algorithm which was used to model the progressive damage in the porous structure due to cyclic loading included the following steps:

1) Define the elastic-plastic material properties of the parent material;
2) Create the geometry of the porous structure; mesh the struts using beam elements with different cross-section areas. Choose the strut diameters from a Gaussian distribution (21 different random cross-section diameters);

3) Constrain the lowermost part of the lattice structure in the Y direction;
4) Define a damage table for each element. This damage table consists of three columns: the element number, the damage in the local y direction of the element (D_y), and the damage in the local z direction of the element (D_z);
5) For the first simulation step, set the cycle increment to $\Delta n_1 = 10$ and set the externally applied displacement to 0.05% of the height of the specimen;
6) In the first simulation step, assign the elastic modulus of the parent material $E = E_s$ to all the struts. In the next simulation steps, depending on the extent of damage in each strut, assign the corresponding decreased elastic modulus. Apply the external compressive displacement to the uppermost nodes of the structure and solve the problem;
7) Find the reaction force of the lattice structure from the lowermost nodes of the structure;
8) Determine whether or not the applied displacement induces the desired stress value to the structure for a stress-controlled analysis. In order to do this, check the difference between the obtained reaction force (obtained in Step 7) and the desired applied force. If the difference is larger than 1%, change the applied displacement and go to Step 6, otherwise go to the next step;
9) Find the bending and axial stresses in each element. Then, calculate the maximum and minimum stresses in each strut by adding and subtracting the bending and axial stresses;
10) Determine the absolute values of stress on the external surface of each strut (in both the local y and z directions). Using the absolute values of stress, calculate the equivalent reversible stress σ_{rev} for each strut in both the local y and z directions (see Note 1 below for σ_{rev});

11) Consider the effect of stress concentration factor on the stress value by multiplying the obtained σ_{rev} by K_f (in both the local y and z directions);

12) Determine the damage caused to each element by the imposed equivalent reversible stress calculated in Step 11. In order to do this:

    a. if the obtained equivalent reversible stress in the local y direction of an element is larger than the endurance limit and less than the intersection stress, use the S-N curve in the high-cycle regime and the Miner's rule (see Note 2 below) to find the damage caused to each element and then sum it up with the previous value of D_y; repeat this for all elements;

    b. if the calculated equivalent reversible stress in the local y direction of an element is larger than the intersection stress and smaller than S_u, use the S-N curve in the low cycle regime and the Miner's rule to find the damage caused to each element, and then sum it up with D_y; repeat this for all elements;

    c. if the equivalent reversible stress or the maximum stress (calculated in Step 9) in the local y direction of an element is larger than S_u, remove the element from the simulation (Note 3 below explains how elements are removed from the simulation).

    d. repeat Steps a-c for the local z direction.

13) If either D_z or D_y value of an element is larger than one, remove it.

14) If the number of failed struts in the simulation cycle is larger than 0.05% of the total number of elements, decrease Δn_{i+1} to $\Delta n_i/5$. If the number of failed struts is smaller than 0.01% of the total number of elements, increase Δn_{i+1} to $\Delta n_i \times 2$.

15) If the number of degraded struts in the simulation cycle is larger than 0.5% of the total number of elements, decrease Δn_{i+1} to $\Delta n_i/5$. If the number of degraded struts is smaller than 0.1% of the total number of elements, increase Δn_{i+1} to $\Delta n_i \times 2$.

16) If the calculated elastic modulus of the lattice structure is smaller than 10% of its initial value, stop the solution, otherwise go to Step 6.

Note 1: The S-N curve data points are usually obtained for completely reversible stresses. In our study, the imposed loading is not completely reversible and is compressive-compressive (with loading ratio $R = 0.1$), which is known as a fluctuating stress. In order to calculate the fatigue life for a fluctuating stress, an *equivalent* reversible stress must be found which causes a damage level similar to the corresponding fluctuating stress. The *equivalent* reversible stress can be found using a modified version of the Goodman's relationship [37, 38]

$$\sigma_{rev} = \frac{\sigma_a}{1 - \frac{\sigma_m}{S_u}} \tag{2}$$

where σ_a and σ_m are the amplitude and mean values of the fluctuating stress, respectively. In this study, $\sigma_{min} = 0.1\,\sigma_{max}$ was considered in accordance with the experimental tests. Therefore, $\sigma_a = \left(\frac{0.9}{2}\right)\sigma_{max}$, and $\sigma_m = \left(\frac{1.1}{2}\right)\sigma_{max}$, then:

$$\sigma_{rev} = \frac{0.45\,\sigma_{max}}{1 - \frac{0.55\,\sigma_{max}}{S_u}} \tag{3}$$

Note 2: In order to find the damage accumulated in each strut during each simulation cycle Δn_i, the Miner's rule [39]

$$D = \sum_i \frac{\Delta n_i}{N_i} \tag{4}$$

was used. To do this, the value of the equivalent reversible stress was calculated for each strut. Then, the life of the strut considering the imposed stress level was calculated (N_i) using the S-N curve of the parent material. After that, the additional damage to each strut was calculated using $\frac{\Delta n_i}{N_i}$.

Note 3: In the FE code, instead of removing an element, its elastic modulus was set to 1 Pa. The extent of damage in the lattice structure was then easier to be visualized;

Note 4: In order to account for the effect of stress concentration factor, the slope of the LogS-LogN diagram must be reduced linearly from $(0, \log S_u)$ to the beginning of endurance limit. In other words, the LogS-LogN curve must have no reduction in its value at S_u, and it needs to have its largest reduction at the endurance limit. Using the downward shifted curve in a LogS-LogN diagram is easy and the equation of the shifted curve can be simply obtained by multiplying the original LogS-LogN curve by a linear equation. However, in order to implement the Miner's rule in our problem, it is necessary to use the shifted LogN-LogS diagram other than the shifted LogS-LogN, i.e. the stress must be the independent variable (or the horizontal axis of the diagram), while the life must be the dependent variable (or the vertical axis of diagram). In the LogN-LogS diagram, the curve needs to be shifted to the left rather than downwards which is customary in the LogS-LogN diagrams. Determining the equation of the shifted LogN-LogS curve is not as easy as the shifted LogS-LogN curve. Here, we explain how the effect of stress concentration factor (which causes leftward shift in the LogN-LogS curve) has been applied in the FE code. If we define T as the logarithmic value of S, i.e. $T = LogS$, and consider K_f as a linear function of $T = logS$, i.e. $K_f(T) = aT + b$ [40], the coefficients a and b can be found using the boundary points:

$$\begin{cases} K_f = 1 & at \quad S = S_u \quad or \quad T = T_u \\ K_f = K_{f,max} & at \quad S = S_e \quad or \quad T = T_e \end{cases} \tag{5}$$

Then:

$$a = \frac{1-K_{f,max}}{T_e - T_u} \quad \text{and} \quad b = 1 - aT_e \tag{6}$$

where $T_u = \log(S_u)$ and $T_e = \log(S_e)$. The shifted value of T in the LogN-LogS diagram due to the effect of stress concentration factor $K_f(T)$ is given by:

$$T_{shifted} = K_f(T).T = aT^2 + bT \tag{7}$$

As explained above, since the FE code needs life as a function of the stress value, the coordinates of the given S-N curve must be interchanged, and the N-S diagram needs to be mapped in the horizontal direction rather than in the vertical direction (see Figure 4). Let us assume that the curve $M = f(T)$ which gives the logarithmic life of the parent material as a function of stress value *without considering* the stress concentration factor is available from experimental tests (Figure 4). Assume that the new logN-LogS curve relating the life to the stress value *considering* the stress concentration factor has the functional form $M = g(T)$ (Figure 4). Here, the problem is to find the fatigue life M_1 corresponding to an arbitrary stress value $T_1 = log(S_1)$ (Figure 4), when an "explicit" form of $M = g(T)$ is not available. Therefore, here we try to find an explicit formula for $M = Log\ (N)$ (Figure 4). We already know that (Figure 4)

$$\begin{cases} M_1 = f(T_2) \\ M_1 = g(T_1) \\ T_1 = K_f T_2 \end{cases} \tag{8}$$

Equating the first and the second lines of Equation (8) gives $g(T_1) = f(T_2)$, which after inserting T_1 from the third line of Equation (8) becomes $g(K_f T_2) = f(T_2)$ which after considering Equation (7) gives

$$g(aT_2^2 + bT_2) = f(T_2) \tag{9}$$

After some algebraic manipulations to simplify the terms inside the parenthesis of the left side of Equation (9), the life of the parent material considering the effect of stress concentration factor is given by:

$$g(T_2) = f\left(\frac{-b + \sqrt{b^2 + 4aT_2}}{2a}\right)$$

or (10)

$$g(T) = f\left(\frac{-b + \sqrt{b^2 + 4aT}}{2a}\right)$$

Combining all the relationships, the life of a material, having the stress level of S and the stress concentration factor $K_{f,max}$ can be found as:

$$N = 10^{f\left(\frac{-b+\sqrt{b^2+4aLog(S)}}{2a}\right)} \tag{11}$$

where $= \frac{1-K_{f,max}}{T_e - T_u}$, $b = 1 - aT_e$, $T_u = \log(S_u)$, $T_e = \text{Log}(S_e)$, and function f is the equation describing the original LogN-LogS curve (which is the logarithmic N-S curve).

2.4. Experimental data

The experimental data from one of our previous studies [15] on the static and fatigue behavior of porous rhombic dodecahedron structures made of Ti6Al4V-ELI was used to validate the computational results obtained in the current study. In that experimental study, porous titanium structures were manufactured using selective laser melting on top of a solid titanium substrate in an inert atmosphere. Four different porous structures with porosities between 66% and 83% were manufactured and their S-N curves were obtained (Table 2). All the specimens had a cylindrical shape with a diameter of $10\ mm$ and length of $15\ mm$. The static tests were carried out using an

INSTRON 5985 testing machine (30 kN load cells) and were done in accordance with the ISO 13314:2011 standard. An MTS hydraulic test machine was used for cyclic compression-compression tests. The applied loads were sinusoidal with a frequency of 15 Hz and load ratio R = 0.1.

3. RESULTS

3.1. Elastic properties

Similar to the experimental observations, the numerical elastic modulus decreased as the porosity of the porous structure increased (Table 3). For all the porous structures, the computationally calculated values of the elastic modulus were between the analytical and experimental values (Table 3). The numerical elastic moduli were generally lower than the analytical values and somewhat higher than the experimental values (Table 3).

3.2. Fatigue

3.2.1. Optimum Δn

The simulation results showed that the resulted plots including the elastic modulus vs. cycle number, the number of removed elements vs. cycle number, and the displacement vs. cycle number diagrams coincide for different Δn_i values, only if in each solution cycle, Δn_i is chosen in such a way that the number of removed elements (in case the elastic modulus degradation is not considered in the analysis) is lower than 0.05% of the total number of elements, or the number of degraded elements (in case the elastic modulus degradation is considered in the analysis) is lower than 0.5% of the total number of elements. Using Δn_is larger than the two aforementioned values led to castellations in the elastic modulus, applied displacement, and number of removed elements diagrams. Furthermore, using large Δn_is, the catastrophic failure of the porous structure usually happened much earlier than expected. In fact, the obtained

displacement and elastic modulus digarams became bilinear, while they were expected to be curved according to the experimental observations. Using very large Δn_is resulted in predicted lives that were even less than 10% of the life calculated using sufficiently small Δn_is.

3.2.2 The effects of manufacturing irregularities

When the irregularities in the cross-section areas of the struts caused by the additive manufacturing process were taken into account in the FE model, the elastic modulus of the Ti 230-500 porous structure decreased by 14.5% (Table 4). The fatigue life of the same porous structure decreased by 72%, 47%, and 35% for the stress levels $\sigma/\sigma_y = 0.2$, $\sigma/\sigma_y = 0.4$ and $\sigma/\sigma_y = 0.6$, respectively (Table 4). Therefore, implementing the manufacturing irregularities in the numerical model affected the fatigue life more severely for the lower levels of applied stress (Table 4).

3.2.3. The effects of stress concentration factor

In order to demonstrate the effects of K_f on the fatigue life of the porous structures for each stress level, the K_f value was varied and the corresponding fatigue life was obtained for Ti 120-500 porous structure (Figure 5). Increasing the stress concentration factor values decreased the obtained fatigue life specially for smaller values of K_f (Figure 5). While the minimum stress concentration factor $K_f = 1$ led to finite life for $\sigma/\sigma_y = 0.4$ and $\sigma/\sigma_y = 0.6$, all K_f values lower than 2.2 led to unlimited fatigue life for $\sigma/\sigma_y = 0.2$ (Figure 5).

3.2.4. The effects of the deterioration of the elastic properties on fatigue behavior

Taking the degradation of elastic modulus of the struts into account resulted in smoother changes in the imposed grip displacement as well as in the elastic modulus of the lattice structure (Figure 6). Moreover, it caused the damage process to start earlier and to end later leading to longer

predicted fatigue lives (Figure 6). Implementing the degradation of the elastic modulus in the model increased the predicted fatigue lives by 2.2-4.5 times (for different samples).

3.2.5. The effects of initial damage

The fatigue life of the Ti 230-500 porous structure ($K_f = 3.125$) having different extents of initial damage was studied. As expected, increasing the level of initial damage decreased the fatigue life (Figure 7). The critical percentage of initial damage causing the porous structures to fail after just one loading cycle were respectively 37%, 18%, and 5% for the stress levels 0.2, 0.4 and $0.6\sigma_y$ (Figure 7). All the curves showed a neck in their middle part which was more pronounced for the cases with lower stress levels (Figure 7).

3.2.6. Results of the fine-tuned fatigue models

The evolution of top grip displacement vs. loading cycle (Figure 8) showed a multi-stage behavior that is typical for porous biomaterials [15, 16]. In the first stage, the displacement changed slowly and there was minimal accumulation of displacement. In the second stage, the displacement increased very rapidly and the specimen failed within a limited number of cycles.

The same two-stage behavior was observed for the evolution of the elastic modulus vs. loading cycle (Figure 9). The evolution of the *normalized* elastic modulus (E/E_0) vs. normalized loading cycle is compared between different stress levels in Ti 230-500 porous structure in Figure 10. The degradation of the elastic modulus started earlier for the case with the highest stress level (Figure 10). Moreover, the curve corresponding to the highest stress level, i.e. $0.6\sigma_y$, had a sharper neck at the final stages of damage (Figure 10), while the curves corresponding to the stress levels $0.2\sigma_y$ and $0.4\sigma_y$ were more or less similar (Figure 10).

The evolution of the number of removed elements vs. loading cycle (Figure 11) also showed the same two-stage behavior observed for the elastic modulus and displacement (Figure 8-10).

Numerical analyses of the different porous structure and stress levels showed that the static failure of the struts usually happen at the very final stages of the collapse of the lattice structure. Ti 230-500 (the densest specimen), however, showed a more gradual static failure of struts.

While the fatigue-life method (S-N diagram, Figure 3) led to acceptable results (Figure 12) for all the stress levels smaller than $0.6\sigma_y$, at stress levels $0.65 - 0.75\sigma_y$ it predicted fatigue lives that were much shorter than what was found experimentally [15]. For stress levels higher than $0.8\sigma_y$, the simulations stopped due to prediction of catastrophic failure at the initial loading cycles.

4. DISCUSSIONS

4.1. Computational costs

The fatigue behavior of porous biomaterials is important for applications where these materials need to sustain many cycles of loading. An obvious example is treatment of large load-bearing bony defects where the bone substituting biomaterial will be subjected to many cycles of loading per day until the bone regeneration has progressed well enough to (partially) unburden the biomaterial. The magnitude of the cyclic load could be as high as several times the body weight [41, 42]. From previous studies on the fatigue behavior of additively manufactured porous biomaterials [14, 15], we know that the fatigue behavior of porous biomaterials is very complex and a function of several factors including not only porosity but also the type of the repeating unit cell used for the design of the porous structure.

These complexities mean a separate study of the fatigue behavior is required for any new design of porous biomaterials, e.g. a new type of unit cell. To study the fatigue behavior of porous biomaterials for design purposes, one often needs to determine the S-N curves corresponding to the different porosities and stress levels of any new type of porous structure [14, 15].

Experimentally determining the S-N curves are generally time-consuming and expensive, as a large number of porous specimens need to be additively manufactured, characterized using advanced imaging techniques, and be tested for a large number of hours.

In the current study, we tried to predict the S-N curve of porous structures given the design of the porous structure (i.e. the type of repeating unit cell and the dimensions of the unit cell) and the S-N curve of the parent material. Given the above-mentioned challenges associated with experimental study of the fatigue behavior of porous biomaterials, the approach presented in the current study is a very attractive approach to predict the S-N curves of any new type of porous structures without having to go through all the required experimental steps. There are, however, two major questions associated with the presented approach. The first question relates to the accuracy of the predictions: is the presented approach capable of providing us with reasonably accurate S-N curves? The results of the current study suggest that the computationally predicted S-N curves are quite close to the one determined experimentally. The second questions relate to the computational cost of predicting the S-N curves using the approach presented here: what are the computational costs associated with predicting the S-N curves of the porous structures? Indeed, the calculations required for any single point of the S-N curves took between 2 hours (for $\sigma/\sigma_y = 0.6$) to 40 hours (for $\sigma/\sigma_y = 0.2$) on a standard personal computer (Core i7 CPU, 6 GB RAM). The computational costs are therefore quite substantial. However, both computational time and the associated costs are estimated to be a small fraction of the costs of a similar experimental study. Nevertheless, computational cost is a strong function of the number of elements used in the FE models. For example, doubling the number of elements (e.g. Ti 170-450 with 27,834 elements as compared to Ti 170-500 with 14,488 elements) quadrupled the computational time.

One way to reduce the computational time required for creating, solving, and analyzing large porous structures is the use of concurrent multi-scale FE models. The micro-struts can be created only in some portions of the structure which are more critical and stress levels are higher. In places where the stress level or stress gradient is lower, relatively large simple solid volume polyhedral elements (such as cubic or tetrahedral elements) can be used to reduce the overall number of elements in the structure. However, special care must be taken when transferring the interfacial stresses and displacements between the models at the micro and macro scales.

4.2. Effect of irregularities

The simulations results showed that considering the irregularities caused by the additive manufacturing process significantly influences the fatigue behavior of the porous structures. In all the cases, considering the irregularities weakened the structures. Taking the irregularities into account decreased the elastic modulus by 10-20% and the fatigue life by 30-70%. A similar decrease in the elastic modulus is reported in [32]. The irregularities decreased the fatigue life more significantly at lower stress levels, because many struts which have been otherwise experiencing stresses below the endurance limit of the parent material experience stresses above their endurance limit when the irregularities are taken into account. That is not the case for the higher stress levels, because for the higher stress levels most struts are already experiencing stresses above their endurance limit.

45^{o} failure bands was formed in both regular and irregular lattice structures after being loaded in cyclic loading. By applying irregularity in the cross-section areas of the struts, this 45^{o} failure bands became more vague (Figure 13). This is because when the initial struts start to fail and as a result are removed from the analysis, the load applied to their neighbour struts start to increase and that makes the failure pattern grow around the initialy failed struts as nucleuses. The

catastrophic failure, however, was formed on almost planar 45º bands. In higher imposed stress levels, the catastrophic failure occurred with lower percentage of struts failed due to fatigue loading.

4.3. Stress concentration factor

The concept of implementing stress concentration factors in calculation of the maximum stress level in the struts of open-cell structures under fatigue loading is used in the current study for the first time. In previous works which modelled the response of open-cell structures under fatigue loading, e.g. [13] and [29], K_f was not used. Numerical simulations on different structure types (Table 2) with random roughness distributions resulted in average stress concentration factors between 3.5 and 5.5 (Table 5). The obtained K_fs are relatively high, because the open-cell microstructures created using the additive manufacturing techniques generally have surface roughnesses with relatively large dimensions (it can be as large as 30% of the strut diameter, see Table 2). Similar large stress concentration effects have been reported in other studies. For example, experimental tests carried out on tubular structures made using SLM technique have shown that the irregularities on the surface of SLM open-cell structures can decrease the fatigue endurance limit to small values of about 50-60 MPa for grade 2 titanium (about one fifth of its initial value) [13]. Experimental K_f values of about 2.2 for roughness values of about $1/10$ of the strut diameters have also been reported in [43].

It is beneficial for the future studies to know with what K_f values the predicted S-N curves are the closest to the experimentally determined S-N curves. The K_f values which were found for the samples studied in this paper conformed to the following equation:

$$K_f = 1 + 0.93\frac{L}{D}\left(1 + \frac{\delta D}{D}\right) \tag{12}$$

where D, L, and δD are the strut nominal diameter, strut nominal length, and standard deviation of the strut diameter in the additively manufactured structure. According to Equation (12), K_f decreases by increasing the strut diameter D. Strut length had an inverse effect, i.e. increasing the strut length increased the K_f value.

4.4. Displacement-N and S-N curves

Experimental tests [15, 16] have shown a three-stage displacement curve (stage I for $1 \leq N \leq 10$, stage II for $10 \leq N \leq 10^3 - 10^5$, and stage III for $10^3 - 10^5 \leq N$. In the first stage, the displacement varies slowly until the start of the second stage. In the second stage, the displacement amplitude remains almost constant, and in the final stage, the displacement increases exponentially until the porous structure fails catastrophically. However, the displacement vs. cycle number plots obtained from our numerical simulations did not exhibit the first stage. Even in the experimental tests, not all the test samples showed the first stage in their displacement-cycle diagrams (for example the displacement-cycle diagrams related to the Ti 120-500 sample at stress levels $0.2\sigma_y$, $0.4\sigma_y$, and $0.6\sigma_y$ which was used as the experimental curve in Figure 6 did not indicate the first stage). Since not all the samples and not all the stress levels show the first stage, the existence of first stage in the experimental curves seems to be a result of test condition rather than actual physical properties of the specimens. A factor which seems to be important in creation of this stage is the preliminary failure of the struts located at the upper and lower surfaces of the open-cell structure. Those struts are not surrounded by adjacent struts and, as a result, are weaker. In those struts, plasticity is the failure mechanism at the very early cycle numbers which leads to an increase in the displacement slope.

The simulations showed that in all the considred porous structure types (Table 2) and regardless of the stress level, the structure fails catastrophically shortly after the number of failed elements

has reached 1% of the total number of elements. After that moment, the accumulated damage in the remaining struts rapidly reaches the failure criteria. However, it was shown that applying intrinsic initial damage has much less effect on the fatigue life of the structure (Figure 7). A similar result for initial damage was shown in [29].

While the fatigue-life method (S-N diagram in Figure 3) led to acceptable results for stress levels lower than $0.6\sigma_y$, it predicted unrealistically short lives for stress levels $0.65 - 0.75\sigma_y$. The displacement-cycle diagrams corresponding to stress levels above $0.6\ \sigma_y$ were not also similar to the experimentally reported curves. That is why the results corresponding to stress levels above $0.6\ \sigma_y$ are not reported in Figure 12. At stress levels larger than $0.8\sigma_y$, the simulation stopped due to prediction of catastrophic failure at the very initial cycles. Since for larger stress levels plasticity becomes important, it seems that other fatigue methods such as strain-life method may need to be used. In that case, a strain-life diagram of the parent material (for example Ti6Al4V) is required.

4.5. Applications in biomedical implants

The bone-mimicking biomaterials studied here need to satisfy several criteria in order to be successfully used in the human body. One of those criteria is appropriate elastic modulus . That criterion is largely satisfied, because the elastic moduli of the porous structures (Table 3) are in the range of those measured for the human bone [44, 45]. There are, however, other criteria related to the fatigue life that need to be also taken into account. Depending on the time it takes for the bone to regenerate inside the porous structure, the number of loading cycles that the porous biomaterials should sustain could be different. Assuming that the number of steps taken per day is a good indicator of the number of loading cycles for the lower extremity applications, the number of steps per month could amount to 150,000 for sedentary individuals, to 225,000 for

lightly active individuals, and to 300,000 for active individuals. The above-mentioned figures are based on the number of steps per day reported in [46]. Since patients receiving bone implants are not likely to be highly active in the first few months after surgery, the loading cycles that the bone substituting material needs to sustain in the first months after surgery is estimated to be between 100,000 and 1,000,000. The bone substituting material should therefore be designed such that it could sustain that many number of cycles. Based on the results obtained in the current study as well as in our previous experimental studies [14, 15], the nominal stress of the porous structure should not be much higher than 20% of the yield stress of the porous structure to ensure the fatigue life reaches the above-mentioned numbers. On the other hand, one crucial factor is not taken into account in these calculations. Bone regenerates into the porous structure, meaning that gradually a higher portion of the mechanical load goes through the regenerated bone and not the implant. In that sense, the estimations presented here are conservative estimations of the fatigue life and the tolerable level of stress in the porous structures. In the future studies, it is suggested that the effects of bone regeneration on the mechanical behavior of porous structures be systematically studied, for example, using a second material that mimics the regenerated bone and gradually fills the pores of the bone substituting biomaterial.

A generic loading scenario is used in most experimental and computational studies of the fatigue behavior of the porous biomaterials. To better resemble the actual loading conditions experienced by the porous biomaterials when used in the human body, it might be more appropriate to use more realistic loading patterns such as the ones predicted using large-scale musculoskeletal models [47, 48] or at least mass-spring-damper models of the human body [49, 50].

4.6. S-N curve of parent material

The S-N curve of the parent material (here Ti6Al4V) is dependent on the processing conditions. The S-N curve of SLM material could be different from the wrought material. Additionally, the microstructure and mechanical properties of SLM materials with different processing parameters (laser power, laser scanning speed, etc.) could be also quite different. In that sense, the S-N curve should be ideally measured for the bulk material of every SLM material with a specific set of processing parameters. In the current study, however, we have been mostly focused on presenting the methodology required for predicting the S-N curve of additively manufactured porous structures from the S-N curve of the bulk material. In the presented methodology, the S-N curve of the bulk material is one of the inputs of the problem. Since extensive information regarding the S-N curves of SLM solid materials is not currently available in the open literature, we have used the S-N curve of the same alloy produced using a different technique. The computational predictions of the S-N curve of the porous material, however, match the experimental values in the particular case of the current study. Even though this may not necessarily be the case for all instances where the S-N curve of additively manufactured porous materials needs to be predicted.

5. CONCLUSIONS

A computational approach for prediction of the fatigue behavior of additively manufactured porous structures was presented in the current study. The computational model could successfully predict the S-N curve of the porous structures for different porosities when the applied stress level did not exceed 60% of the yield stress. The presented model was not very successful for higher stress levels and underestimated the fatigue life. Moreover, considering manufacturing irregularities substantially reduced the fatigue lives of the FE porous structures. The level of decrease was particularly high for lower stress levels. The simulations showed that

in all the considred porous structure types and regardless of the stress level, the structure fails catastrophically shortly after the number of failed elements has reached 1% of the total number of elements. After that moment, the accumulated damage in the remaining struts rapidly reaches the failure criteria. However, it was shown that applying intrinsic initial damage has much less effect on the fatigue life of the structure.

REFERENCES

1. Bates, P. and M. Ramachandran, *Bone injury, healing and grafting.* Basic Orthopaedic Sciences. The Stanmore Guide, 2006: p. 123-134.
2. Dimitriou, R., G.I. Mataliotakis, A.G. Angoules, N.K. Kanakaris, and P.V. Giannoudis, *Complications following autologous bone graft harvesting from the iliac crest and using the RIA: a systematic review.* Injury, 2011. **42**: p. S3-S15.
3. Van der Stok, J., O.P. Van der Jagt, S. Amin Yavari, M.F. De Haas, J.H. Waarsing, H. Jahr, E.M. Van Lieshout, P. Patka, J.A. Verhaar, and A.A. Zadpoor, *Selective laser melting‐produced porous titanium scaffolds regenerate bone in critical size cortical bone defects.* Journal of Orthopaedic Research, 2013. **31**(5): p. 792-799.
4. Hedayati, R., M. Sadighi, M. Mohammadi-Aghdam, and A.A. Zadpoor, *Mechanics of additively manufactured porous biomaterials based on the rhombicuboctahedron unit cell.* Journal of the Mechanical Behavior of Biomedical Materials, 2016. **53**: p. 272–294.
5. Hedayati, R., M. Sadighi, M. Mohammadi-Aghdam, and A.A. Zadpoor, *Mechanical properties of regular porous biomaterials made from truncated cube repeating unit cells: analytical solutions and computational models.* Materials Science and Engineering: C, 2015. **Accepted**.
6. Amin Yavari, S., S. Ahmadi, J. van der Stok, R. Wauthlé, A. Riemslag, M. Janssen, J. Schrooten, H. Weinans, and A.A. Zadpoor, *Effects of bio-functionalizing surface treatments on the mechanical behavior of open porous titanium biomaterials.* Journal of the mechanical behavior of biomedical materials, 2014. **36**: p. 109-119.
7. Van der Stok, J., M. Koolen, M. De Maat, S. Amin Yavari, J. Alblas, P. Patka, J. Verhaar, E. Van Lieshout, A. Zadpoor, and H. Weinans, *Full regeneration of segmental bone defects using porous titanium implants loaded with BMP-2 containing fibrin gels.* European Cells & Materials, 2015. **29**: p. 141-153.
8. Heinl, P., C. Körner, and R.F. Singer, *Selective electron beam melting of cellular titanium: mechanical properties.* Advanced Engineering Materials, 2008. **10**(9): p. 882-888.
9. Traini, T., C. Mangano, R. Sammons, F. Mangano, A. Macchi, and A. Piattelli, *Direct laser metal sintering as a new approach to fabrication of an isoelastic functionally graded material for manufacture of porous titanium dental implants.* Dental materials, 2008. **24**(11): p. 1525-1533.
10. Mullen, L., R.C. Stamp, W.K. Brooks, E. Jones, and C.J. Sutcliffe, *Selective Laser Melting: A regular unit cell approach for the manufacture of porous, titanium, bone in‐growth constructs, suitable for orthopedic applications.* Journal of Biomedical Materials Research Part B: Applied Biomaterials, 2009. **89**(2): p. 325-334.
11. Salmi, M., K.-S. Paloheimo, J. Tuomi, J. Wolff, and A. Mäkitie, *Accuracy of medical models made by additive manufacturing (rapid manufacturing).* Journal of Cranio-Maxillofacial Surgery, 2013. **41**(7): p. 603-609.
12. SU, X.-b., Y.-q. YANG, Y. Peng, and J.-f. SUN, *Development of porous medical implant scaffolds via laser additive manufacturing.* Transactions of Nonferrous Metals Society of China, 2012. **22**: p. s181-s187.
13. Lipinski, P., A. Barbas, and A.-S. Bonnet, *Fatigue behavior of thin-walled grade 2 titanium samples processed by selective laser melting. Application to life prediction of porous titanium implants.* Journal of the mechanical behavior of biomedical materials, 2013. **28**: p. 274-290.
14. Amin Yavari, S., S. Ahmadi, R. Wauthle, B. Pouran, J. Schrooten, H. Weinans, and A. Zadpoor, *Relationship between unit cell type and porosity and the fatigue behavior of selective laser melted meta-biomaterials.* Journal of the mechanical behavior of biomedical materials, 2015. **43**: p. 91-100.

15. Amin Yavari, S., R. Wauthlé, J. van der Stok, A. Riemslag, M. Janssen, M. Mulier, J.-P. Kruth, J. Schrooten, H. Weinans, and A.A. Zadpoor, *Fatigue behavior of porous biomaterials manufactured using selective laser melting.* Materials Science and Engineering: C, 2013. **33**(8): p. 4849-4858.
16. Sugimura, Y., A. Rabiei, A. Evans, A. Harte, and N. Fleck, *Compression fatigue of a cellular Al alloy.* Materials Science and Engineering: A, 1999. **269**(1): p. 38-48.
17. Banhart, J. and W. Brinkers, *Fatigue behavior of aluminum foams.* Journal of materials science letters, 1999. **18**(8): p. 617-619.
18. Zhou, J. and W. Soboyejo, *Compression–compression fatigue of open cell aluminum foams: macro-/micro-mechanisms and the effects of heat treatment.* Materials Science and Engineering: A, 2004. **369**(1): p. 23-35.
19. McCullough, K., N. Fleck, and M. Ashby, *The stress-life fatigue behaviour of aluminium alloy foams.* Fatigue and Fracture of Engineering Materials and Structures, 2000. **23**(3): p. 199-208.
20. Motz, C., O. Friedl, and R. Pippan, *Fatigue crack propagation in cellular metals.* International journal of fatigue, 2005. **27**(10): p. 1571-1581.
21. Harte, A.-M., N. Fleck, and M. Ashby, *Fatigue failure of an open cell and a closed cell aluminium alloy foam.* Acta materialia, 1999. **47**(8): p. 2511-2524.
22. Leuders, S., M. Thöne, A. Riemer, T. Niendorf, T. Tröster, H. Richard, and H. Maier, *On the mechanical behaviour of titanium alloy TiAl6V4 manufactured by selective laser melting: Fatigue resistance and crack growth performance.* International Journal of Fatigue, 2013. **48**: p. 300-307.
23. Barriuso, S., J. Chao, J. Jiménez, S. García, and J. González-Carrasco, *Fatigue behavior of Ti6Al4V and 316 LVM blasted with ceramic particles of interest for medical devices.* Journal of the mechanical behavior of biomedical materials, 2014. **30**: p. 30-40.
24. Mangipudi, K. and P. Onck, *Multiscale modelling of damage and failure in two-dimensional metallic foams.* Journal of the Mechanics and Physics of Solids, 2011. **59**(7): p. 1437-1461.
25. Lipperman, F., M. Ryvkin, and M.B. Fuchs, *Nucleation of cracks in two-dimensional periodic cellular materials.* Computational Mechanics, 2007. **39**(2): p. 127-139.
26. Lee, S.-J., J. Wang, and B.V. Sankar, *A micromechanical model for predicting the fracture toughness of functionally graded foams.* International journal of solids and structures, 2007. **44**(11): p. 4053-4067.
27. Choi, S. and B.V. Sankar, *A micromechanical method to predict the fracture toughness of cellular materials.* International journal of solids and structures, 2005. **42**(5): p. 1797-1817.
28. Ableidinger, A., *Some aspects of the fracture behavior of metal foams*. 2000: na.
29. Demiray, S., W. Becker, and J. Hohe, *Investigation of the fatigue behavior of open cell foams by a micromechanical 3-D model.* Materials Science and Engineering: A, 2009. **504**(1): p. 141-149.
30. Hedayati, R., M. Sadighi, M. Mohammadi-Aghdam, and A. Zadpoor, *Mechanical behavior of additively manufactured porous biomaterials made from truncated cuboctahedron unit cells.* Submitted, 2015.
31. Hedayati, R., M. Sadighi, M. Mohammadi-Aghdam, and A.A. Zadpoor, *Effect of mass multiple counting on the elastic properties of open-cell regular porous biomaterials.* Materials & Design, 2015. **5**: p. 9–20.
32. Campoli, G., M. Borleffs, S. Amin Yavari, R. Wauthle, H. Weinans, and A.A. Zadpoor, *Mechanical properties of open-cell metallic biomaterials manufactured using additive manufacturing.* Materials & Design, 2013. **49**: p. 957-965.
33. Shigley, J.E., R.G. Budynas, and C.R. Mischke, *Mechanical engineering design.* 2004.
34. Lemaitre, J., *A continuous damage mechanics model for ductile fracture.* Journal of Engineering Materials and Technology, 1985. **107**(1): p. 83-89.
35. Lemaitre, J. and H. Lippmann, *A course on damage mechanics*. Vol. 2. 1996: Springer Berlin.
36. Alves, M.l., J. Yu, and N. Jones, *On the elastic modulus degradation in continuum damage mechanics.* Computers & Structures, 2000. **76**(6): p. 703-712.
37. Goodman, J., *Mechanics applied to engineering*. 1919: Longmans, Green.
38. *Goodman relation.* 2015; Available from: http://en.wikipedia.org/wiki/Goodman_relation.
39. Miner, M.A., *Cumulative damage in fatigue.* Journal of applied mechanics, 1945. **12**(3): p. 159-164.
40. Stephens, R.I., A. Fatemi, R.R. Stephens, and H.O. Fuchs, *Metal fatigue in engineering*. 2000: John Wiley & Sons.
41. Nikooyan, A.A. and A.A. Zadpoor, *Effects of muscle fatigue on the ground reaction force and soft-tissue vibrations during running: a model study.* Biomedical Engineering, IEEE Transactions on, 2012. **59**(3): p. 797-804.

42. Shelburne, K.B., M.R. Torry, and M.G. Pandy, *Contributions of muscles, ligaments, and the ground‐reaction force to tibiofemoral joint loading during normal gait.* Journal of orthopaedic research, 2006. **24**(10): p. 1983-1990.
43. Hasan, R., *Progressive collapse of titanium alloy micro-lattice structures manufactured using selective laser melting*. 2013, University of Liverpool.
44. Zysset, P.K., X.E. Guo, C.E. Hoffler, K.E. Moore, and S.A. Goldstein, *Elastic modulus and hardness of cortical and trabecular bone lamellae measured by nanoindentation in the human femur.* Journal of biomechanics, 1999. **32**(10): p. 1005-1012.
45. Kaneko, T.S., M.R. Pejcic, J. Tehranzadeh, and J.H. Keyak, *Relationships between material properties and CT scan data of cortical bone with and without metastatic lesions.* Medical engineering & physics, 2003. **25**(6): p. 445-454.
46. Tudor-Locke, C. and D.R. Bassett Jr, *How many steps/day are enough?* Sports Medicine, 2004. **34**(1): p. 1-8.
47. Lloyd, D.G. and T.F. Besier, *An EMG-driven musculoskeletal model to estimate muscle forces and knee joint moments in vivo.* Journal of biomechanics, 2003. **36**(6): p. 765-776.
48. Pandy, M.G., *Computer modeling and simulation of human movement.* Annual review of biomedical engineering, 2001. **3**(1): p. 245-273.
49. Nikooyan, A.A. and A.A. Zadpoor, *An improved cost function for modeling of muscle activity during running.* Journal of biomechanics, 2011. **44**(5): p. 984-987.
50. Zadpoor, A.A. and A.A. Nikooyan, *A mechanical model to determine the influence of masses and mass distribution on the impact force during running—a discussion.* Journal of Biomechanics, 2006. **39**(2): p. 388-390.
51. Ahmadi, S., G. Campoli, S. Amin Yavari, B. Sajadi, R. Wauthlé, J. Schrooten, H. Weinans, and A. Zadpoor, *Mechanical behavior of regular open-cell porous biomaterials made of diamond lattice unit cells.* Journal of the mechanical behavior of biomedical materials, 2014. **34**: p. 106-115.
52. Babaee, S., B.H. Jahromi, A. Ajdari, H. Nayeb-Hashemi, and A. Vaziri, *Mechanical properties of open-cell rhombic dodecahedron cellular structures.* Acta Materialia, 2012. **60**(6): p. 2873-2885.

List of figure captions

List of table captions

List of tables

Table 1- Mechanical properties of Ti6Al4V [15, 51]

Property	**Value**
Elastic modulus	122.3 GPa
Poisson's ratio	0.342
Tangent modulus	1.25 GPa
Yield stress	1000 MPa
Ultimate tensile strength	1200 MPa

Table 2- Geometrical specifications of the four simulated samples [15]

	Ti 120-500	**Ti 170-450**	**Ti 170-500**	**Ti 230-500**
Dimensions D×L (mm×mm)	10×15	10×15	10×15	10×15
Porosity (%)	83.7 ± 0.3	70.1 ± 0.3	77.1 ± 0.5	66.4 ± 0.3
Nomianl pore size (µm)	500	450	500	500
Nominal strut size (µm)	120	170	170	230
Actual pore size (µm)	560±173	486±162	608±182	560±186
Actual strut size (µm)	140±38	216±64	218±62	251±76

Table 3- Comparison of the analytical, numerical, and experimental values of elastic modulus for different samples

	Ti 120-500	**Ti 170-450**	**Ti 170-500**	**Ti 230-500**
Analytical solution (MPa) [52]	621	5241	2412	5324
FE modeling (MPa)	584	3155	2195	4598
Experiment (MPa) [15]	550	2620	1400	3490

Table 4- Effect of considering irregularity on the elastic modulus and fatigue life of Ti 230-500 porous structure ($K_f = 3.125$)

	Elastic modulus (MPa)	**Life ($\sigma/\sigma_y = 0.2$)**	**Life ($\sigma/\sigma_y = 0.4$)**	**Life ($\sigma/\sigma_y = 0.6$)**
Regular lattice	5372	1350000	46240	9681
Irregular lattice	4598	383637	24340	6250

Table 5- Values of stress concentration factor for the four FE models

	$\frac{\delta D}{D}$	$\frac{L}{D}$	K_f
Ti 120-500	0.271	4	5.55
Ti 170-450	0.296	2.27	3.57
Ti 170-500	0.284	2.8	4.34
Ti 230-500	0.302	2.23	3.525

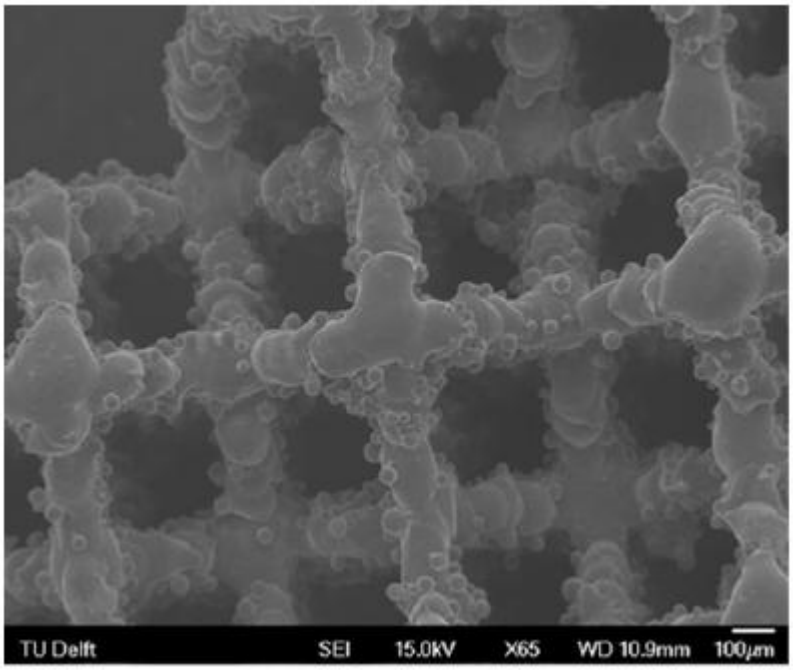

(a)

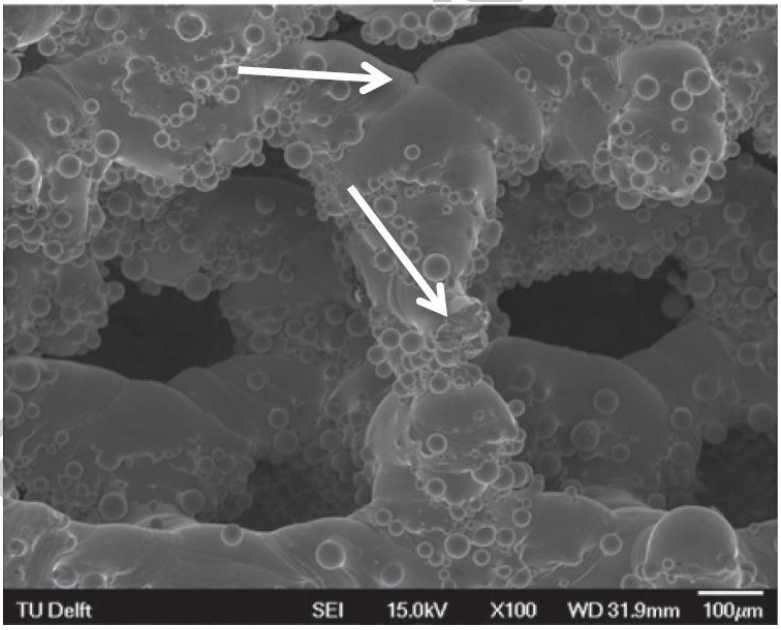

(b)

Figure 1- The struts of a sample porous material manufactured using selective melting (a) X65 scale, and (b) X100 scale [15, 32]. The arrows identify some crack initiation sites with potentially high stress values.

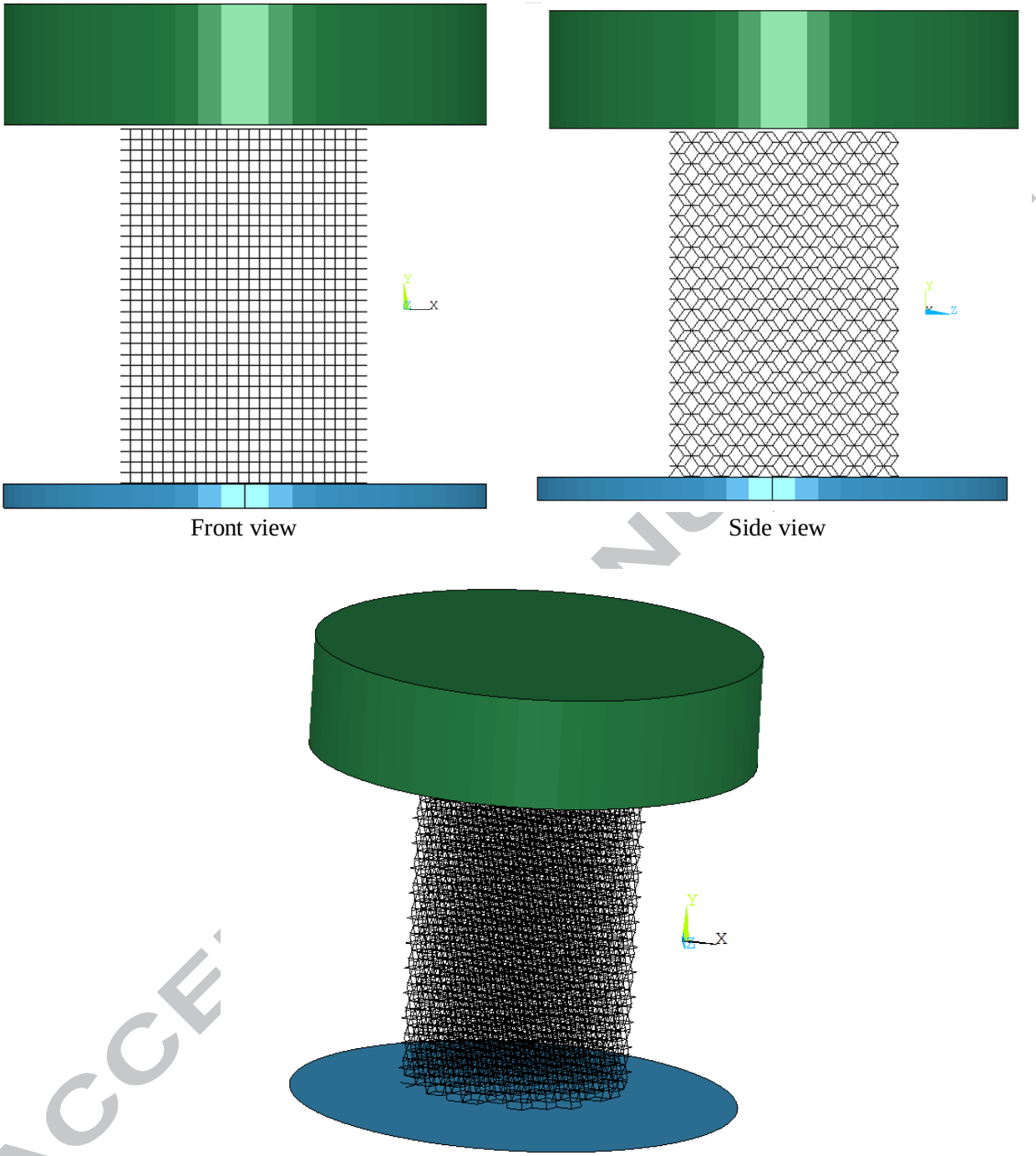

Front view

Side view

3D view

Figure 2- FE model of the rhombic dodecahedron structure from different views

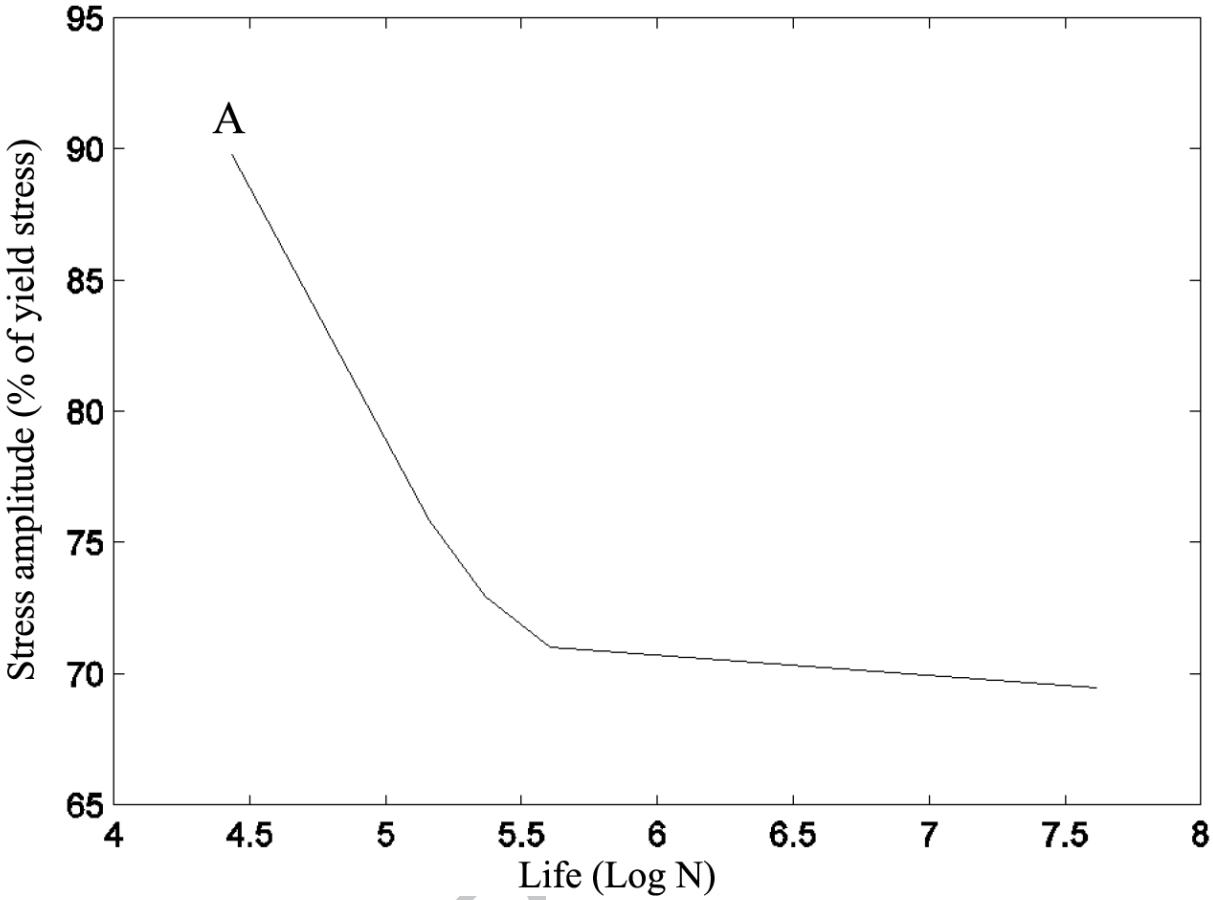

Figure 3- The S-N curve used for describing the fatigue behaviour of the parent material in the FE solution [23]

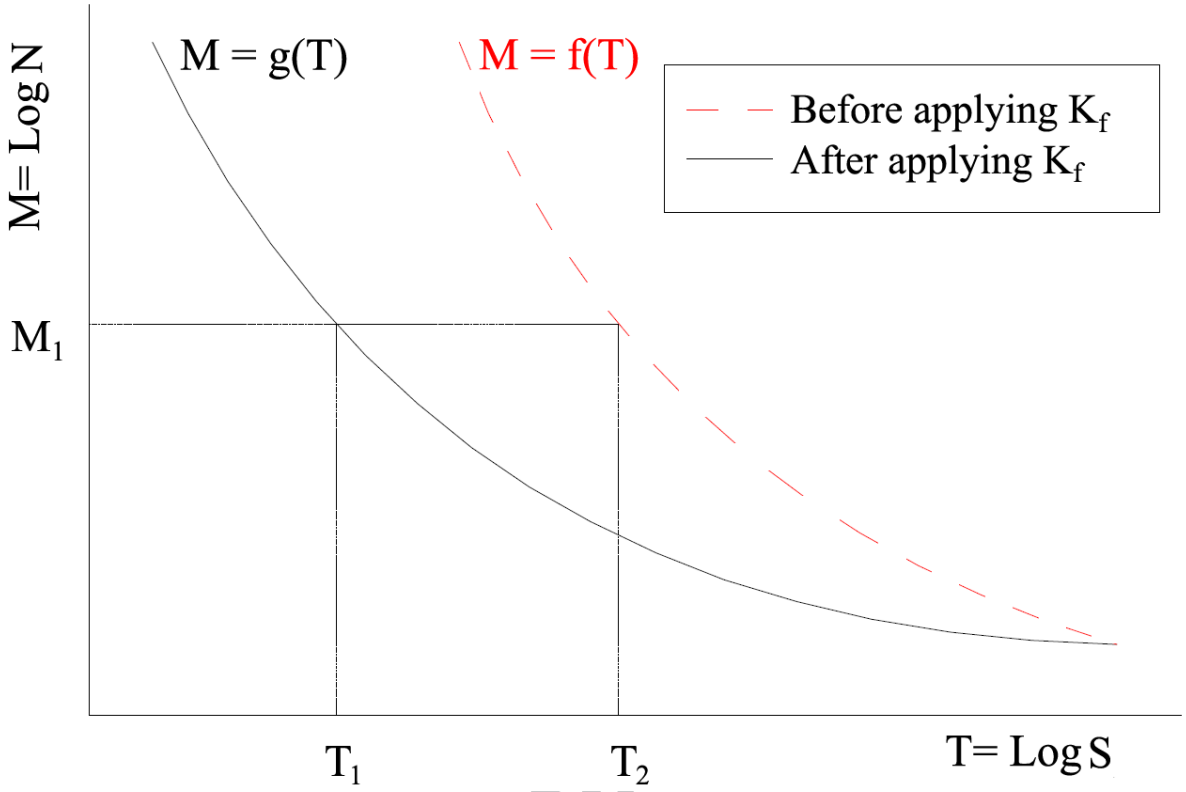

Figure 4- The shift of a typical LogN-LogS curve to left after applying the stress concentration factor effect

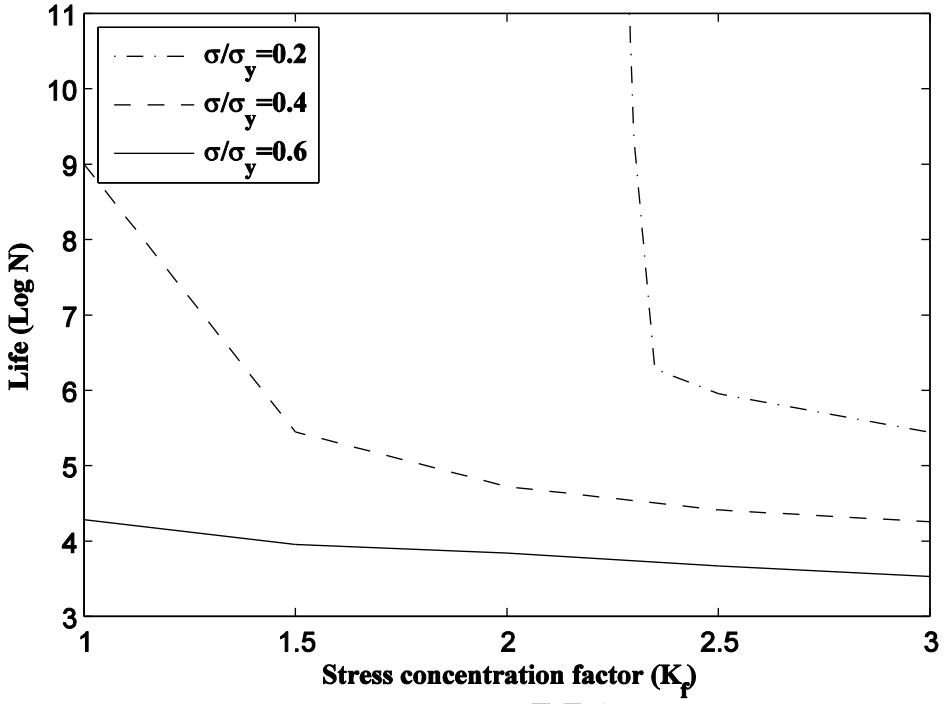

Figure 5- Effect of K_f on the fatigue life of Ti 120-500 lattice structure in different stress levels

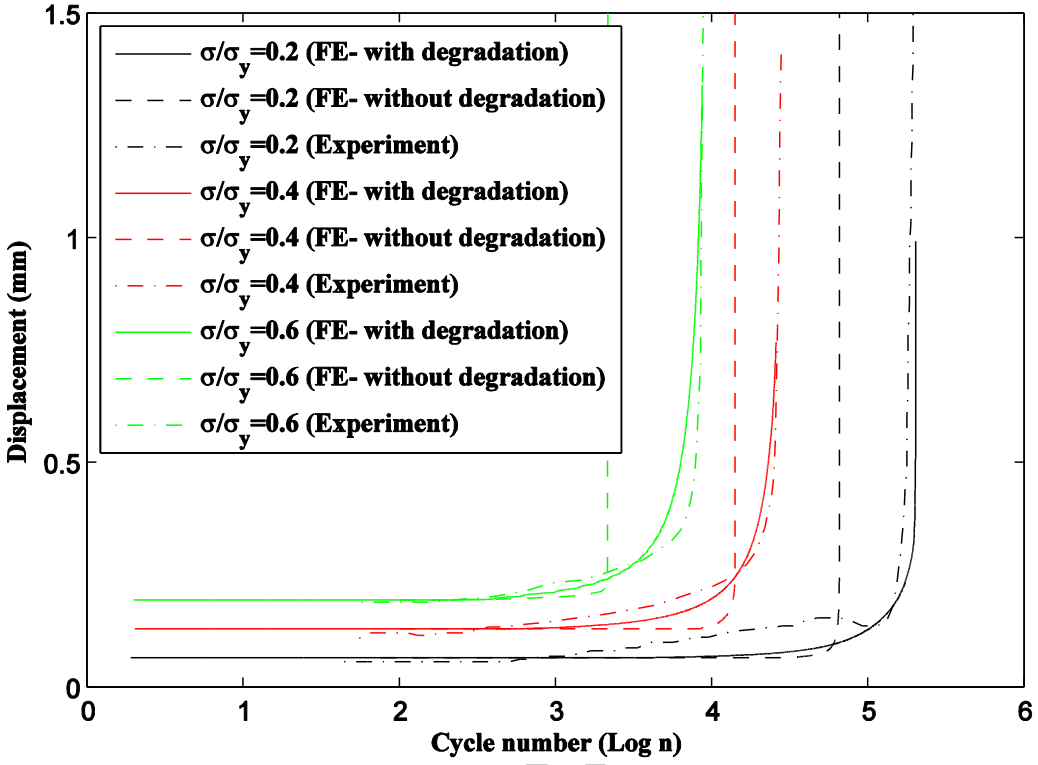

(a)

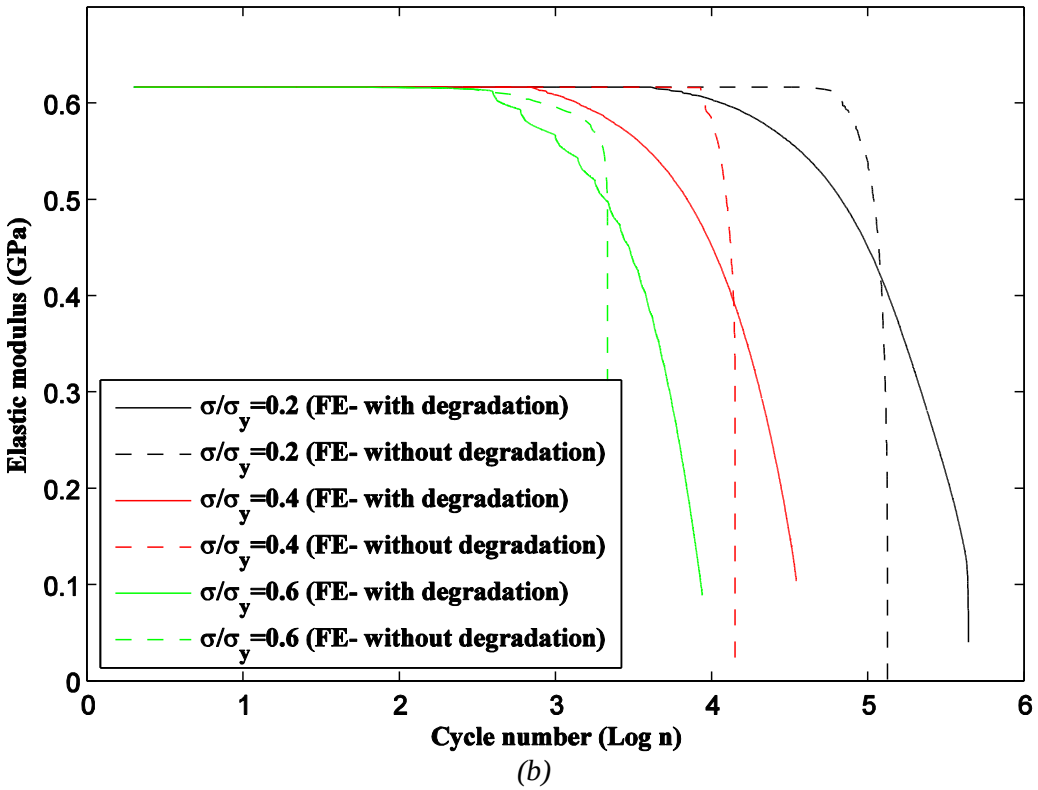

(b)

Figure 6- Effect of consideration of elastic modulus degradation on the variations of (a) imposed displacement on the lattice structure, and (b) lattice structure elastic modulus

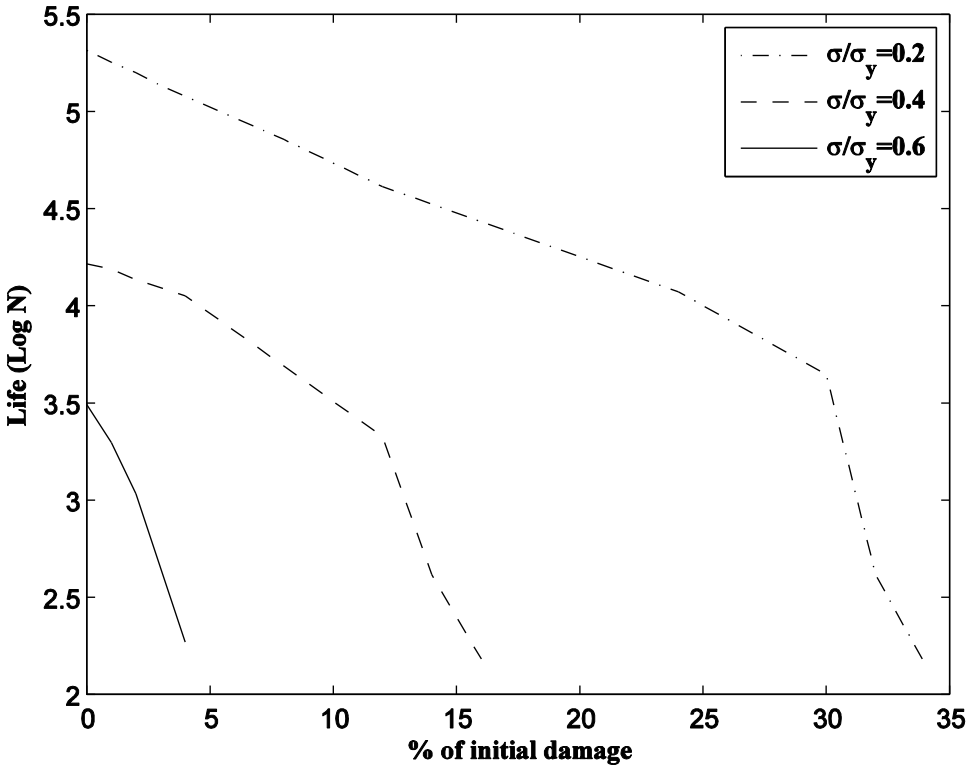

Figure 7- Effect of initial damage on the fatigue life of Ti 230-500 sample for different stress levels

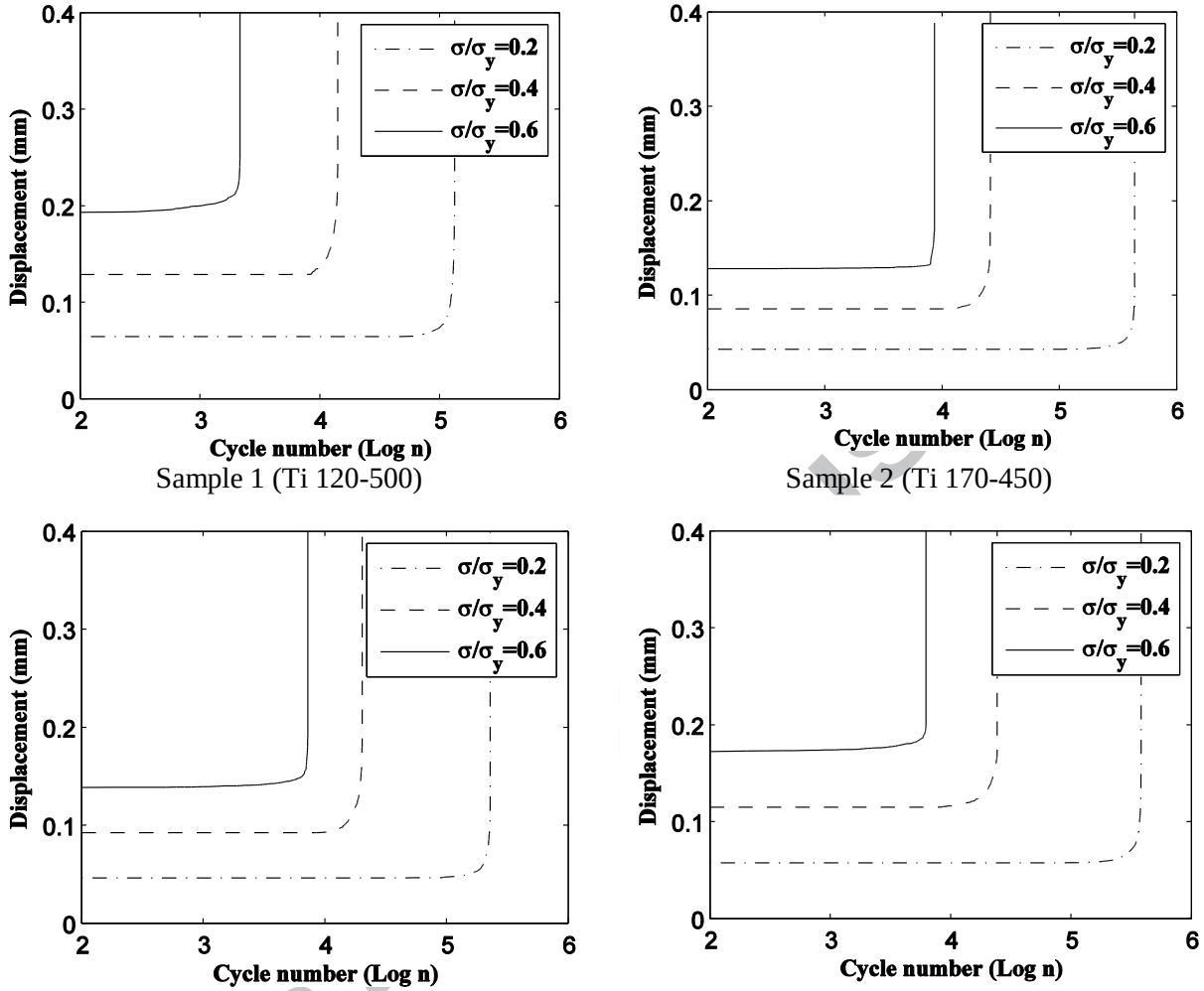

Sample 1 (Ti 120-500) Sample 2 (Ti 170-450)

Sample 3 (Ti 170-500) Sample 4 (Ti 230-500)

Figure 8- Variation of the top grip displacement vs. cycle number for the four samples at different imposed stress levels

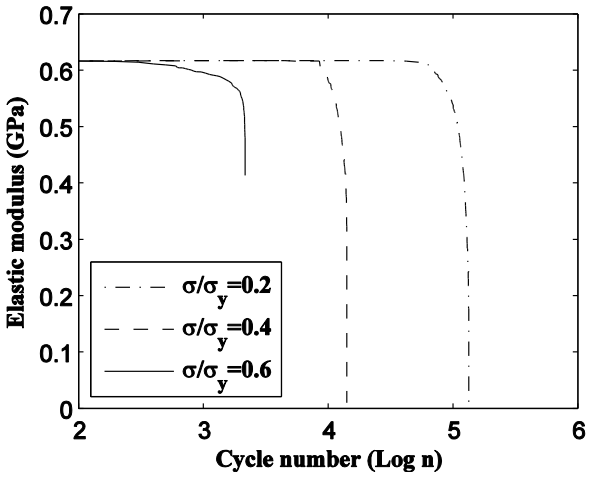

Sample 1(Ti 120-500)

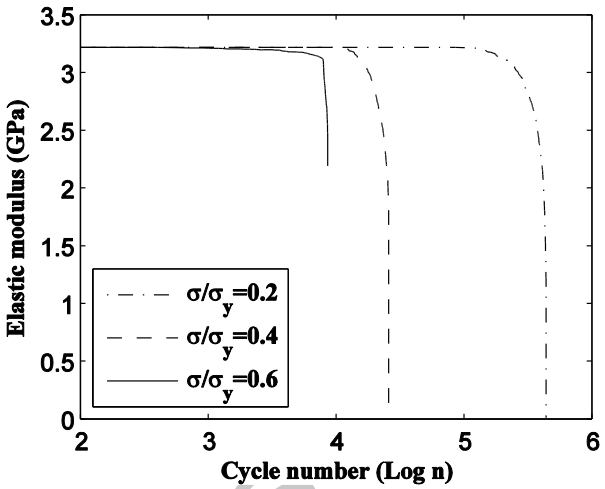

Sample 2 (Ti 170-450)

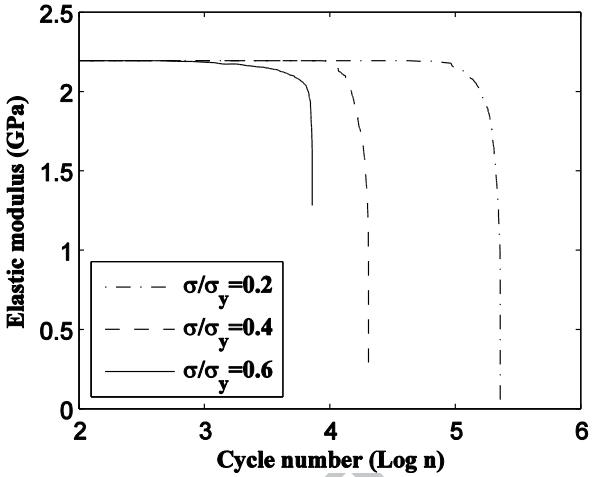

Sample 3 (Ti 170-500)

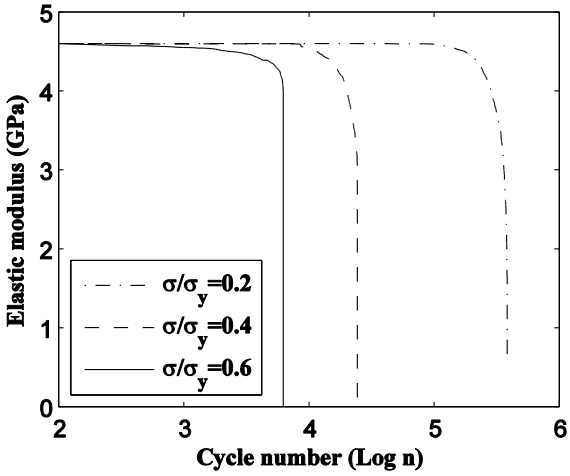

Sample 4 (Ti 230-500)

Figure 9- Variation of the elastic modulus vs. cycle number for the four samples at different imposed stress levels

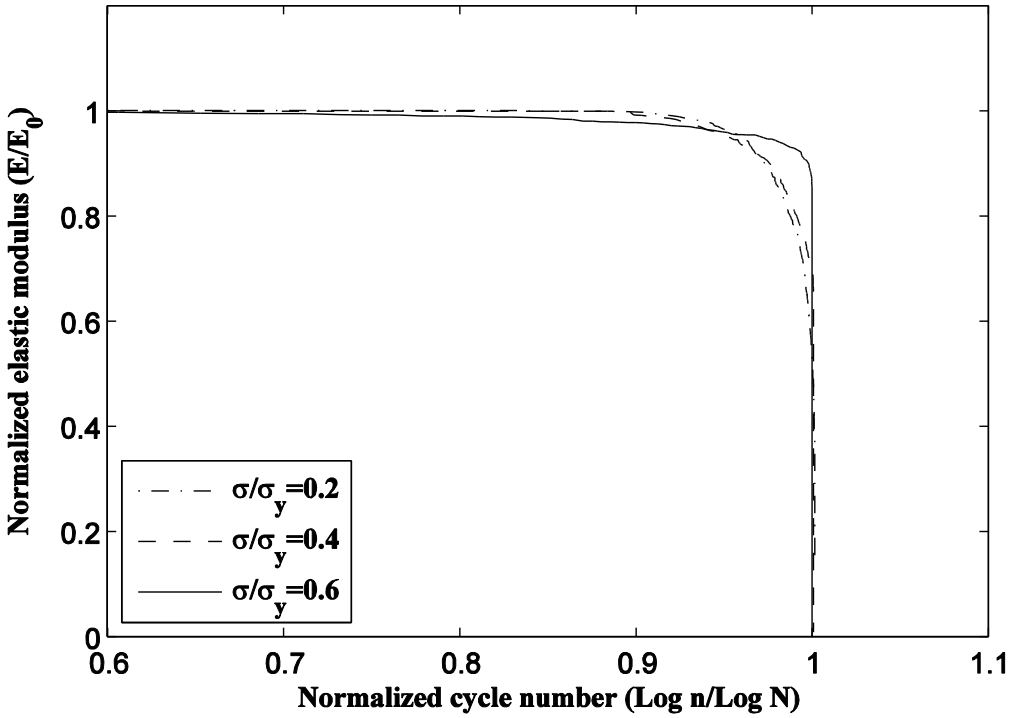

Figure 10- Variation of the normalized elastic modulus vs. normalized cycle number for sample Ti 230-500 at different stress levels

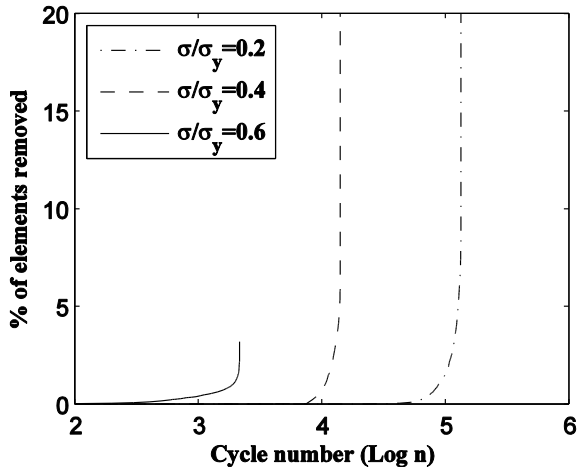

Sample 1 (Ti 120-500)

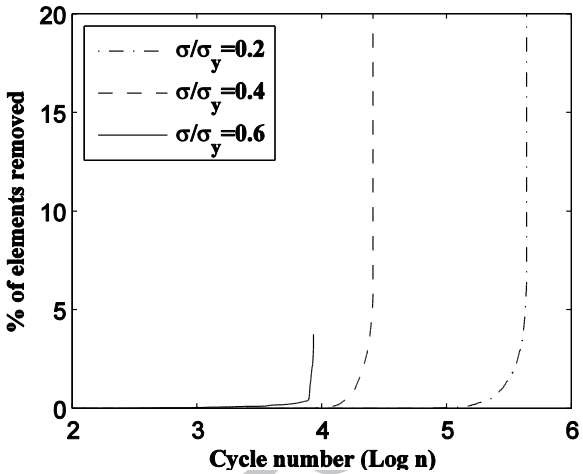

Sample 2 (Ti 170-450)

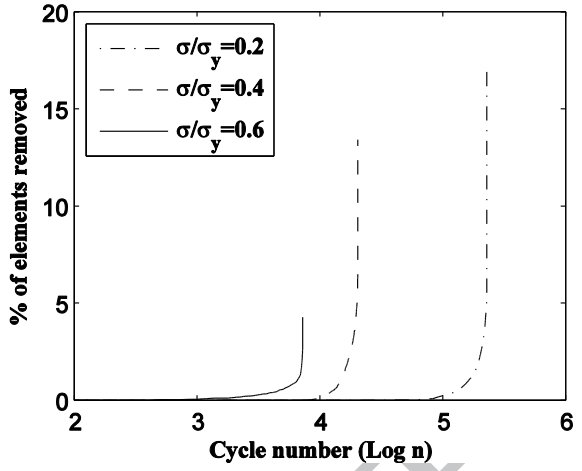

Sample 3 (Ti 170-500)

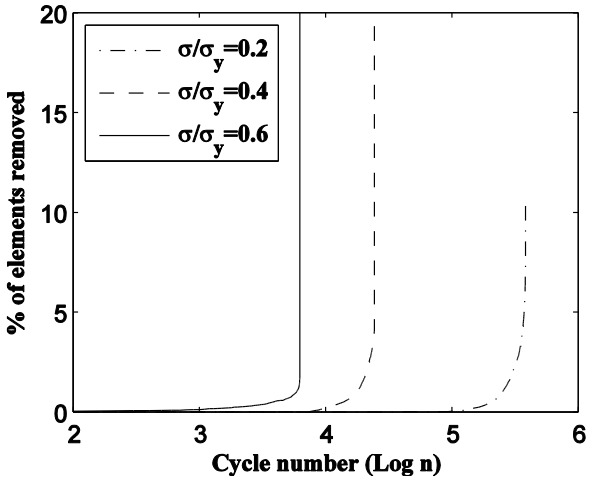

Sample 4 (Ti 230-500)

Figure 11- Variation of the elements removed vs. cycle number for the four samples at different imposed stress levels

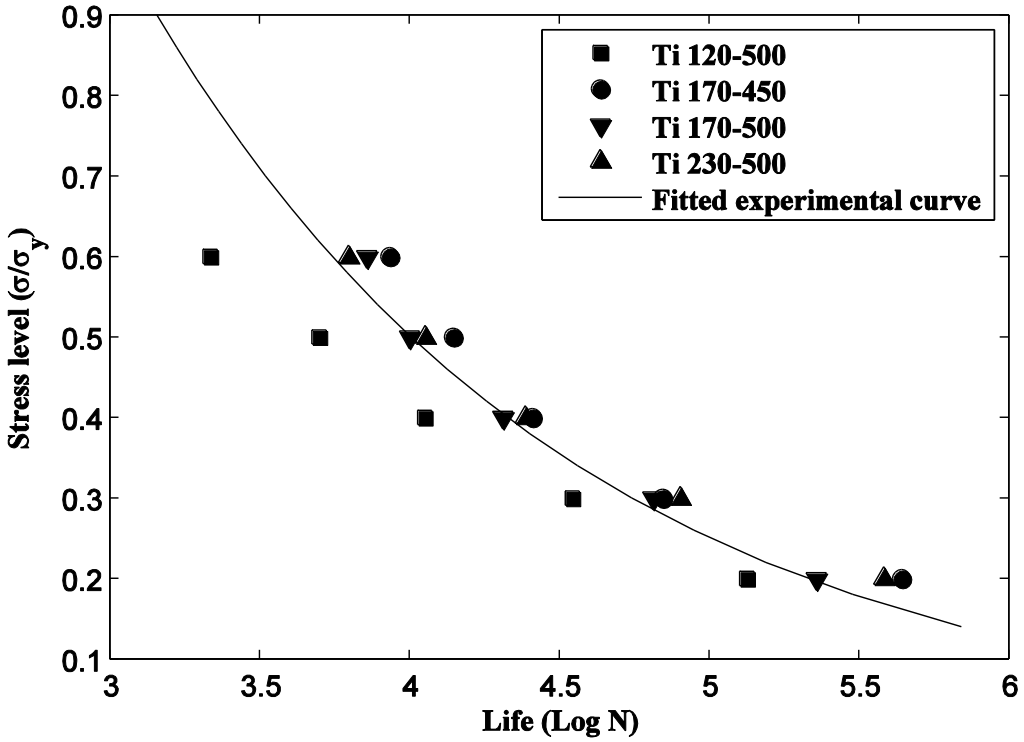

Figure 12- Stress level vs. Log N data points for the four FE models compared to the experimental curve [32]. The experimental curve is a power law fitted to all data points of the normalized experimental S–N curves.

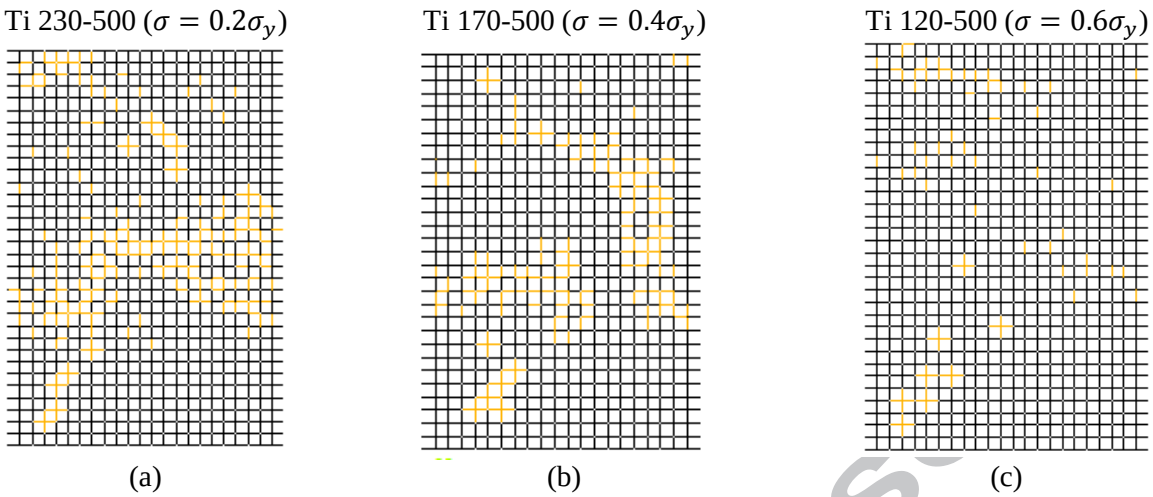

Figure 13- The failed struts at the final stages of fatigue failure for some samples and stress levels

Highlights

- An FE approach for prediction the fatigue behavior of porous structures is presented.
- The FE model could successfully predict the S-N curve of the porous structures.
- Considering manufacturing irregularities reduced the fatigue life.
- The structures failed catastrophically shortly after 1% of elements had failed.
- Applying initial damage has much less effect on the fatigue life of the structure.